Magnetic resonance of type-I fcc antiferromagnets

Marko T. Heinilä* and Aarne S. Oja†
Low Temperature Laboratory, Helsinki University of Technology, 02150 Espoo, Finland
(Received 24 May 1996)

We calculate magnetic-resonance absorption curves for an assembly of classical spins located in an fcc lattice with spin-spin interactions which stabilize antiferromagnetic order of the first kind. The only source of anisotropy in the model is the dipole-dipole interaction which, at equilibrium, confines the ordered moments into planes perpendicular to the respective type-I ordering vectors. Our principal tool of analysis combines numerical integration of the equations of motion with Monte Carlo simulations. Complete absorption line shapes for classical spins can be calculated using this technique. Spin dynamics is investigated as well by extending our earlier mean-field analysis, the results of which are compared with the simulations. Special attention is paid to a sum rule that relates the intensities of the resonance peaks to the static susceptibility. To this end, we calculate the static susceptibility matrixes for certain single-**k** and triple-**k** type-I structures. We investigate, in particular, examples of cases where thermal fluctuations beyond the mean-field theory shift resonance lines from zero frequency to a finite value. It is demonstrated that this effect is related to the so-called ''ordering-by-disorder'' mechanism in which fluctuations stabilize a unique ground state in a continuously degenerate manifold. Our results explain several features observed in recent NMR studies of antiferromagnetic nuclear-spin ordering in copper and silver at nanokelvin temperatures. Analogies with spin dynamics in solid ^{3}He and superfluid ^{3}He-*A* are briefly discussed. [S0163-1829(96)06337-0]

I. INTRODUCTION

Spin dynamics in antiferromagnets in an fcc lattice have become a subject of considerable current interest as the result of extensive studies of nuclear magnetic ordering in simple metals such as copper, silver, and rhodium at nanokelvin temperatures.[1] Of particular importance is antiferromagnetic (AF) ordering of the first kind which has been found in copper and silver,[2] and is expected in rhodium.[3] Another interesting aspect of spin dynamics in these systems derives from the inherent frustration in the fcc lattice which leads to extensive ground-state degeneracy. We have recently shown that subtle fluctuation effects, which lift the degeneracy, leave a signature in the nuclear-magnetic resonance signal. Spin dynamics of type-I fcc antiferromagnets have also interesting similarities with superfluid ^{3}He-*A* and solid ^{3}He. These features have provided the general motivation for the present study.

Early evidence of magnetic ordering in copper and silver was obtained from measurements of the dynamic susceptibility in zero external field, or in a low field below the critical value.[1] Characteristic changes were observed in the absorption signal when the system underwent AF ordering. The NMR line shape in the AF state yields information on the symmetry of the spin structure. In special cases, the nature of the magnetic order can be obtained from NMR.[4,5] Such information would be particularly useful for nuclear magnets since neutron-diffraction measurements are exceedingly difficult, albeit feasible in certain cases.[1,2] Until recently,[6] however, analysis of antiferromagnetic NMR spectra of copper and silver has yielded little information on the spin structure. Even some important qualitative features of the AF resonance spectra of copper and silver were not fully understood, such as the number of maxima in the absorption curve.

Although the theory of AF resonance was developed in the 1950's,[7–9] there are several complications which hamper direct application of this early work to the present case. Most of the NMR data on copper and silver were measured in zero external field. As the crystal structure is cubic in these metals, there is no single-spin anisotropy in the Hamiltonian, and the positions of the NMR lines are determined by spin-spin interactions and by the ordered structure. In most electronic systems in which AF resonance has been investigated, the situation is different: Anisotropy caused by noncubic crystal symmetry and/or magnetoelastic effects is important.

A diagonal component of the dynamic susceptibility tensor $\chi(\omega)$ can be written as $\chi(\omega)=\chi'(\omega)+i\chi''(\omega)$, where the complex quantity has been divided into its real and imaginary parts. Energy absorption in an axial radio-frequency field is proportional to the imaginary part $\chi''(\omega)$. In resonance experiments in a low field, however, it is more convenient to look at the *form function* $\chi''(\omega)/\omega$, which is connected to the static susceptibility $\chi'(0)$ through a Kramers-Kroenig relation, viz., $\chi'(0)=(2/\pi)\int_0^\infty \chi''(\omega)d\omega/\omega$. In the paramagnetic state when $B=0$, $\chi''(\omega)/\omega$ peaks at $\omega=0$; such a signal is called zero-frequency resonance. The physical meaning of this response can be illustrated by considering the signal caused by a small steplike change in the external field. When the zero-frequency resonance curve has, for example, the Lorentzian form, the system reacts via a process in which the magnetization relaxes exponentially towards a new equilibrium value, and the relaxation time is essentially the inverse of the linewidth at the $\omega=0$ resonance.

According to measurements on copper[10] and our theoretical work,[6] relaxation in the paramagnetic state becomes more complicated and clearly deviates from a simple shape such as

the Lorentzian when spins are cooled towards the ordering temperature T_N. In the AF state, the line shape undergoes a clear change: $\chi''(\omega)/\omega$ develops a peak, or several peaks, at a finite frequency. These are called AF resonances. At this point, the matrix nature of $\chi(\omega)$ becomes important since the symmetry of $\chi(\omega)$ might be reduced in antiferromagnetic state, and all diagonal components of $\chi(\omega)$ do not necessarily behave in the same way.

The zero-frequency peaks of the paramagnetic state can follow several alternative scenarios below T_N. (i) The peak can shift to higher frequencies to become the AF resonance. (ii) It may stay at $\omega=0$ or, (iii) it it may shift to a low frequency which is, however, clearly below the AF resonance.

The last two scenarios have an interesting relationship with the geometric frustration of the fcc lattice. A consequence of this is that the type-I antiferromagnet shows continuous degeneracy within the mean-field (MF) theory. From this one expects the presence of soft modes, i.e., spin-wave excitations with zero energy. If there are soft modes with a zero wave vector, their presence should be seen by NMR, since this technique probes excitations which have a nonzero magnetization.

In most cases when one might expect a soft mode, we find a peak in the form function at a low but nonzero frequency (see Sec. IV D). This is explained by the presence of an artificial hidden symmetry in the MF Hamiltonian. When fluctuations beyond the MF theory are considered, the $\omega=0$ resonance is found[6] to move to a finite frequency. The effect can be understood in terms of a thermally induced anisotropy field which is also responsible for lifting the ground-state degeneracy. The phenomenon is a manifestation of the so-called order-by-disorder mechanism, introduced by Villain and his co-workers.[11] It has been discussed extensively in the context of ground-state selection in frustrated systems.[12] Appearance of a gap in the magnon dispersion relation at zero wave vector has been investigated previously using neutron scattering in the electronic magnet $Ca_3Fe_2Ge_3O_{12}$.[13]

We have recently employed a numerical method, which combines Monte Carlo simulations and numerical solutions of the equations of motion, to compute complete NMR absorption line shapes.[6,14] In principle, our technique yields complete resonance curves for classical spin systems. In the present paper we show simulated NMR absorption spectra for a model in which the strength of the nearest-neighbor dipolar interaction, with respect to the exchange coupling, is similar to that between nuclear spins in silver. However, the results should illustrate, for a large range of interaction constants, features which cannot be extracted from mean-field calculations. Apart from the type-I ground state, the only essential assumption in our procedure is the sign of the anisotropic spin-spin interaction: The ordered moments are in the plane perpendicular to the type-I ordering vectors.

First, however, we present and extend a previous[15] mean-field description of the AF resonance in type-I fcc antiferromagnets. It is well known that the MF approximation for the dynamics fails in several important respects. For example, the MF theory does not give any information about the shape of the absorption peak. Nevertheless, the MF results are useful as they provide a basis for understanding the salient features of AF resonance curves. By comparing the MF predictions with the simulated results, we can test the reliability of the MF dynamics.

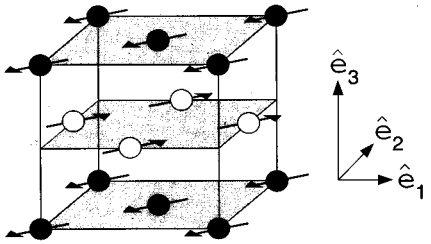

FIG. 1. Illustration of a type-I fcc antiferromagnet. In this single- $\mathbf{k}$ state the ordering vector $\mathbf{Q}=\mathbf{Q}_3=(\pi/a)\hat{\mathbf{e}}_3$. The structure consists of ferromagnetic sheets in which the spins $\langle\mathbf{I}_i\rangle/I$ are either $+\mathbf{d}_3$ or $-\mathbf{d}_3$ in a zero external field. Dipolar anisotropy confines $\mathbf{d}_3$ to the plane perpendicular to $\hat{\mathbf{e}}_3$.

This paper is organized as follows. In Sec. II we discuss the MF theory of the AF resonance in type-I fcc antiferromagnets. The general expressions for the resonance frequencies and their intensities are derived. Special attention is paid to the sum rule which relates the intensities of the resonances at finite frequencies and at $\omega=0$ to the static susceptibility. To this end, we calculate complete static susceptibility matrices for type-I structures. We also briefly discuss similarities between the spin dynamics of type-I antiferromagnets and of solid ^{3}He and superfluid ^{3}He-*A*. In Sec. III we describe specific results for single-$\mathbf{k}$ and a triple-$\mathbf{k}$ structures which are likely candidates for the ground states of copper and silver in certain field regions. In Sec. IV, we present simulated NMR spectra of type-I antiferromagnets. Various components of the absorption matrix are compared with predictions of the MF dynamics. In Sec. V we compare our results with experiments on copper and silver. Details of the calculation of the static susceptibility matrix are presented in the Appendix.

II. MEAN-FIELD THEORY

For the Hamiltonian we assume

$$\mathcal{H}=\sum_{i>j}\sum_{\mu\nu} I_i^{\mu}A_{ij}^{\mu\nu}I_j^{\nu}-\gamma\hbar\mathbf{B}\cdot\sum_i \mathbf{I}_i\,. \tag{1}$$

Here the $\mathbf{I}_i$ are quantum spin operators and the matrix A_{ij} contains the spin-spin interactions which originate from exchange and classical dipole-dipole forces.

A. Statics

Type-I antiferromagnetism in an fcc lattice is characterized by the the spin configurations[15,16]

$$\langle\mathbf{I}_i\rangle/I=\mathbf{m}+\sum_{j=1,2,3}\mathbf{d}_j\cos(\mathbf{Q}_j\cdot\mathbf{r}_i), \tag{2}$$

with the type-I ordering vectors $\mathbf{Q}_j=(\pi/a)\hat{\mathbf{e}}_j$. Here a is one half of the fcc lattice parameter $a_0=(4/\rho)^{1/3}$, and $\rho=N/V$ is the number density of the fcc lattice sites. The three fcc crystal axes are denoted by the unit vectors $\hat{\mathbf{e}}_1$, $\hat{\mathbf{e}}_2$ and $\hat{\mathbf{e}}_3$. As an example, we have illustrated in Fig. 1 one of the possible

single-**k** structures.

According to the mean-field (MF) theory, thermal expectation values of spins are

$$\frac{\langle \mathbf{I}_i \rangle}{I} = \frac{\mathbf{B}_i}{B_i} \mathcal{B}_I\left(\frac{\gamma I \hbar B_i}{k_B T} \right), \tag{3}$$

where $\mathcal{B}_I(x)$ is the Brillouin function and $\mathbf{B}_i$ the average local field

$$B_i^\mu = B^\mu - \frac{1}{\gamma\hbar} \sum_{\nu,j} A_{ij}^{\mu\nu} \langle I_j^\nu \rangle. \tag{4}$$

The Fourier transform of the interaction matrix is defined by

$$\underline{A}(\mathbf{q}) = \sum_j \underline{A}_{ij} \exp[-i\mathbf{q}\cdot(\mathbf{r}_i - \mathbf{r}_j)] \ . \tag{5}$$

It is diagonal for the type-I ordering vectors:

$$\underline{A}(\mathbf{Q}_j) = \lambda \underline{I} + (\lambda_1 - \lambda) \hat{\mathbf{e}}_j \hat{\mathbf{e}}_j \, . \tag{6}$$

We assume $\lambda_1 > \lambda$ which implies an easy-plane anisotropy. As a result, structures with

$$\hat{\mathbf{e}}_j \cdot \mathbf{d}_j = 0 \tag{7}$$

are favored [see Eq. (2)]. Anisotropy is of this type if dipolar forces are the dominant anisotropic spin-spin interactions. This should be the case for copper and silver.[17]

For $\mathbf{q}=0$ one finds

$$\underline{A}(\mathbf{0}) = \lambda_0 \underline{I} \tag{8}$$

if the sample is assumed to be spherical; in this case only exchange forces contribute to λ_0.

For the spin structure of Eq. (2), the static susceptibility χ_0 parallel to the static magnetic field is[15]

$$\chi_0 = \mu_0 \rho \gamma I \hbar / B_c, \tag{9}$$

which does not depend on temperature or magnetic field in the AF phase. Here B_c is the zero-temperature critical field for type-I antiferromagnetism

$$B_c = (I/\gamma\hbar)(\lambda_0 - \lambda). \tag{10}$$

Calculation of the full static susceptibility matrix $\underline{\chi}(\omega=0)$ is somewhat complicated, mostly due to the degeneracy of the MF ground states. While $\underline{\chi}(\omega=0)$ for a single-**k** structure can be obtained, with some modifications, from the work by Van Vleck,[18] it seems that double-**k** and triple-**k** structures have not been investigated before. Our calculation of $\underline{\chi}(\omega=0)$ is presented in Appendix I.

The MF ground state of Eq. (2) is continuously degenerate since two components of the $\mathbf{d}_j$ vectors are left undetermined. A unique ground state is stabilized by thermal or quantum effects beyond the MF approach.[19]

B. Dynamics

In MF theory, the dynamics is described by

$$\frac{d\langle \mathbf{I}_i \rangle}{dt} = \gamma \langle \mathbf{I}_i \rangle \times \mathbf{B}_i \, . \tag{11}$$

Without time-dependent external fields, Eq. (3) gives the expectation values $\langle \mathbf{I}_i \rangle$. It is impossible to find a consistent solution for the dynamic susceptibility $\underline{\chi}(\omega)$ without considering Eq. (3) and Eq. (11) together, since both are needed to solve the zero-frequency behavior of $\underline{\chi}(\omega)$. This point will be illustrated in Sec. III using the MF theory and in Sec. IV by direct numerical methods based on the linear-response theory.

The equations of motion for $\mathbf{m}$ and $\mathbf{d}_j$, $j=1,2,3$, can be found by Fourier transforming Eq. (11). This yields[15]

$$\frac{1}{\gamma}\frac{d\mathbf{m}}{dt} = \mathbf{m}\times\mathbf{B} - B_D \sum_{j=1,2,3} (\mathbf{d}_j \times \hat{\mathbf{e}}_j)(\hat{\mathbf{e}}_j \cdot \mathbf{d}_j) \tag{12}$$

and

$$\begin{aligned}\frac{1}{\gamma}\frac{d\mathbf{d}_j}{dt} = {} & \mathbf{d}_j \times (\mathbf{B} - B_c \mathbf{m}) - B_D (\mathbf{m}\times\hat{\mathbf{e}}_j)(\hat{\mathbf{e}}_j\cdot\mathbf{d}_j) \\ & - B_D (\mathbf{d}_k \times \hat{\mathbf{e}}_l)(\hat{\mathbf{e}}_l \cdot \mathbf{d}_l) - B_D (\mathbf{d}_l \times \hat{\mathbf{e}}_k)(\hat{\mathbf{e}}_k \cdot \mathbf{d}_k).\end{aligned} \tag{13}$$

In Eq. (13) indices (j,k,l) denote, again, (1,2,3), (2,3,1) or (3,1,2). The coefficient

$$B_D = (I/\gamma\hbar)(\lambda_1 - \lambda), \tag{14}$$

with the dimension of magnetic induction, could be called the anisotropy field for type-I order. When the dipole-dipole interaction is the only anisotropic contribution to spin-spin interactions, the tabulated[20] lattice sums yield, for an fcc lattice, $B_D \approx (\mu_0/4\pi)\rho\gamma I\hbar \times 6.501$.

If only one of the $\mathbf{d}_j$'s is nonzero, Eqs. (12) and (13) are almost identical with those proposed[5] for solid ^{3}He. The difference is that in ^{3}He it is generally possible to neglect the terms proportional to the dipole-dipole energy in Eq. (13) because they are small. This approximation is not needed, however, when equations are solved to the first order in the excitation field,[15] since the same terms disappear anyway. Equations (12) and (13) have also much in common with the Leggett equations[21] of superfluid ^{3}He-*A* if we identify his $\hat{\mathbf{l}}$ and $\mathbf{d}$ with our $\hat{\mathbf{e}}_1$ and $\mathbf{d}_1$. Spin dynamics of ^{3}He-*A* resembles, however, a uniaxial antiferromagnet with an easy axis along $\hat{\mathbf{l}}$. The Leggett equations for a constant $\hat{\mathbf{l}}$ are, therefore, obtained when B_D in Eq. (12) is negative and the B_D terms in Eq. (13) are again ignored. It should be mentioned, however, that the dynamics of easy-plane and easy-axis antiferromagnets with some overlap with the cases discussed here, has been presented earlier using a somewhat different formalism.[7–9]

Assume that a field $\mathbf{B}(t) = \mathbf{B}_0 + \mathbf{B}_1(t)$ is applied on the system. We expand the spin vectors in leading orders of B_1: $\mathbf{m}(t) = \mathbf{m}^{(0)} + \mathbf{m}^{(1)}(t) + O(B_1^2)$ and similarly for $\mathbf{d}_j(t)$. Our aim is to solve for the quantity $\mathbf{m}^{(1)}(t)$ which is of first order in $\mathbf{B}_1(t)$. One obtains from Eq. (13), using Eq. (7)

$$\frac{1}{\gamma}\frac{d}{dt}(\hat{\mathbf{e}}_j\cdot\mathbf{d}_j)=(\hat{\mathbf{e}}_j\times\mathbf{d}_j^{(0)})\cdot(\mathbf{B}_1-B_c\mathbf{m}^{(1)})+O(B_1^2). \quad (15)$$

Combination of this result with Eq. (12) yields

$$\frac{1}{\gamma}\frac{d^2\mathbf{m}^{(1)}}{dt^2}=\mathbf{m}^{(0)}\times\frac{d\mathbf{B}_1}{dt}-\mathbf{B}_0\times\frac{d\mathbf{m}^{(1)}}{dt}-\gamma B_D\sum_{j=1,2,3}(\mathbf{d}_j^{(0)}\times\hat{\mathbf{e}}_j)$$
$$\times(\hat{\mathbf{e}}_j\times\mathbf{d}_j^{(0)})\cdot(\mathbf{B}_1-B_c\mathbf{m}^{(1)}). \quad (16)$$

Introducing the Fourier transformation $f(\omega)=(2\pi)^{-1}\int_{-\infty}^{\infty}f(t)\exp(i\omega t)dt$ and noting that $\mathbf{M}_1(\omega)=\rho\gamma I\hbar\mathbf{m}^{(1)}(\omega)$ and $M_1^{\mu}(\omega)=\Sigma_\nu\chi^{\mu\nu}(\omega)B_1^{\nu}(\omega)/\mu_0$, we find if $\omega\neq 0$,

$$\underline{\chi}_H(\omega)/\chi_0=[\underline{\Upsilon}(\omega)-\underline{I}\omega^2/\gamma B_c]^{-1}\underline{\Upsilon}(\omega), \quad (17)$$

where

$$\underline{\Upsilon}(\omega)=\gamma B_D\sum_{j=1,2,3}(\hat{\mathbf{e}}_j\times\mathbf{d}_j^{(0)})(\hat{\mathbf{e}}_j\times\mathbf{d}_j^{(0)})$$
$$-i\omega\sum_{j=1,2,3}(\mathbf{m}^{(0)}\times\hat{\mathbf{e}}_j)\hat{\mathbf{e}}_j. \quad (18)$$

Subscript ''H'' of $\underline{\chi}_H(\omega)$ in Eq. (17) emphasizes that the theory gives only the non-dissipative part of $\underline{\chi}(\omega)=\underline{\chi}_H(\omega)+\underline{\chi}_{\mathrm{AH}}(\omega)$ since $\underline{\Upsilon}(\omega)$ and the right-hand side of Eq. (17) are Hermitian matrices. This follows since the description without relaxation mechanisms fails exactly at the resonant frequencies.

To obtain $\underline{\chi}_{\mathrm{AH}}(\omega)$ we use a consequence of the Kramers-Kroenig relations, namely

$$\underline{\chi}_{\mathrm{AH}}(\omega)=\frac{1}{i\pi}\mathcal{P}\int_{-\infty}^{\infty}\frac{\underline{\chi}_H(\omega_0)d\omega_0}{\omega_0-\omega}. \quad (19)$$

The rules for constructing $\underline{\chi}_{\mathrm{AH}}(\omega)$ from the poles of $\underline{\chi}_H(\omega)$ are the following:

$$\frac{\Omega^2}{\Omega^2-\omega^2}\rightarrow\frac{i\pi\Omega}{2}[\delta(\omega-\Omega)-\delta(\omega+\Omega)], \quad (20)$$

$$\frac{\Omega\omega}{\Omega^2-\omega^2}\rightarrow\frac{i\pi\Omega}{2}[\delta(\omega-\Omega)+\delta(\omega+\Omega)]. \quad (21)$$

The dynamic susceptibility matrix can be written as

$$\underline{\chi}(\omega)/\chi_0=\frac{1}{2}\sum_\alpha\frac{\underline{\Lambda}_\alpha}{1-\omega/(\Omega_\alpha-i\Gamma_\alpha)}$$
$$+\frac{1}{2}\sum_\alpha\frac{\underline{\Lambda}_\alpha^*}{1+\omega/(\Omega_\alpha+i\Gamma_\alpha)}, \quad (22)$$

where Ω_α is the resonant frequency and the Hermitian matrix Λ_α the resonant amplitude. Equation (17) is the Hermitian part of this expression in the limit $\Gamma_\alpha\rightarrow 0+$ when $\omega\neq 0$. Equation (22) must also contain an appropriate term with zero resonant frequency. The $\Omega=0$ term is of the form

$$\frac{\underline{\Lambda}_0}{1-i\omega/\Gamma_0}$$

and describes a simple exponential relaxation of the induced magnetization. $\underline{\Lambda}_0$ can be calculated from the equation

$$\underline{\chi}(0)/\chi_0=\sum_\alpha\ \mathrm{Re}\{\underline{\Lambda}_\alpha\}, \quad (23)$$

which decomposes the static susceptibility matrix into contributions from various resonances Ω_α. Calculation of $\underline{\chi}(0)$ is discussed in Appendix I. Only do the resonances at $\omega=0$ and at Larmor frequencies $\omega=\gamma B_0$ persist in the disordered state.

III. APPLICATIONS

In the following discussion we write the susceptibility using an orthonormal coordinate system with the basis $(\hat{\mathbf{x}},\hat{\mathbf{y}},\hat{\mathbf{z}})$. We always select $\hat{\mathbf{z}}\|\mathbf{B}_0$. In all cases of interest we can also assume that the spins lie in the yz plane; this fixes our coordinate system with respect to the directions of the spins.

A. Single-k states

It is meaningful to divide single-**k** states into two classes. The zero-field configuration and structures with $\mathbf{Q}_j\|\mathbf{B}_0$ form the first class and can be considered exceptional. All other single-**k** structures fall into the second class. It turns out that $\underline{\chi}(0)$ is anisotropic in the first case and isotropic in the second. MF theory predicts a zero-frequency resonance only for configurations in the first class.

1. B=0 and a field along Q_j

Assume first that $\mathbf{B}_0\geqslant 0$ is along a crystalline axis, say $\hat{\mathbf{z}}=\hat{\mathbf{e}}_3$. We consider a structure with the modulation vector $\mathbf{Q}_3$ which is in the direction of $\mathbf{B}_0$:

$$\mathbf{m}=(B_0/B_c)\hat{\mathbf{e}}_3\|\hat{\mathbf{z}},$$
$$\mathbf{d}_1=\mathbf{d}_2=0,$$
$$\mathbf{d}_3=\pm[p^2-(B_0/B_c)^2]^{1/2}\hat{\mathbf{y}}. \quad (24)$$

Here we assume $B_0\leqslant pB_c$ where pB_c is the critical field for antiferromagnetism at polarization p in the mean-field theory. This configuration is the relevant ground state for a range of spin-spin interaction constants.[1,19] Various calculations indicate that the vector $\mathbf{d}_3$ is either along $\hat{\mathbf{e}}_1$, $\hat{\mathbf{e}}_2$ or $\hat{\mathbf{e}}_1\pm\hat{\mathbf{e}}_2$; our results do not depend, however, on this direction.

The nonzero components of the static susceptibility $\underline{\chi}(0)$ are given by

$$\chi^{xx}(0)=\chi^{zz}(0)=\chi_0, \quad \chi^{yy}(0)=\chi_{yy} \quad (25)$$

with

$$\chi_{yy}/\chi_0=\frac{B_DB_cp^2(1-\tau)+B_0^2\lambda\tau/(\lambda-\lambda_0)}{B_DB_cp^2(1-\tau)+(\Omega_\perp/\gamma)^2\lambda\tau(\lambda-\lambda_0)}. \quad (26)$$

Here $\tau=\tau(p)$ is a monotonous function of polarization defined in Appendix I; in particular, τ assumes the values $\tau(0)=0$ and $\tau(1)=1$. The qualitative behavior at $B_0=0$ is such that χ_{yy} increases from zero at $T=0$ to $\chi_{yy}=\chi_0$ at $T=T_N$.[18] When $B_0\neq 0$, a small external field along the $\hat{\mathbf{y}}$ direction twists $\mathbf{d}_3$ out of the easy plane $\hat{\mathbf{e}}_3\cdot\mathbf{d}_3=0$.

Quantity $\Omega_\perp$ is a resonant frequency, viz.,

$$\Omega_\perp^2/\gamma^2 = B_0^2(1-B_D/B_c) + p^2 B_D B_c . \tag{27}$$

Apart from the $\omega=0$ peak, $\Omega_\perp$ is the only resonance in $\underline{\chi}(\omega)$. The nonzero components of the amplitude $\underline{\Lambda}_\perp$ are

$$\Lambda_\perp^{xx}=1, \quad \Lambda_\perp^{xy}=(\Lambda_\perp^{yx})^*=i\gamma B_0/\Omega_\perp, \quad \Lambda_\perp^{yy}=(\gamma B_0/\Omega_\perp)^2. \tag{28}$$

We have for the $\omega=0$ resonance

$$\Lambda_0^{yy}=\chi_{yy}/\chi_0-(\gamma B_0/\Omega_\perp)^2, \quad \Lambda_0^{zz}=1, \tag{29}$$

and find that Λ_0^{yy} vanishes in the zero-temperature limit when $p\to 1$.

Let us now assume that the structure given by Eq. (24) is actually stabilized by an additional phenomenological anisotropy term $\propto(\mathbf{d}_3\cdot\hat{\mathbf{x}})^2$. This interaction energy can be included in the analysis of Sec. II B by replacing Eq. (6) with

$$\underline{A}(\mathbf{Q}_3)=\lambda\underline{I}+(\lambda_T-\lambda)\hat{\mathbf{x}}\hat{\mathbf{x}}+(\lambda_1-\lambda)\hat{\mathbf{e}}_3\hat{\mathbf{e}}_3, \tag{30}$$

where $\lambda_T>\lambda$. After steps analogous to Eqs. (11)–(18) one finds that the matrix $\underline{\Upsilon}(\omega)$ assumes the form

$$\underline{\Upsilon}(\omega)=\gamma B_D(\hat{\mathbf{e}}_3\times\mathbf{d}_3)(\hat{\mathbf{e}}_3\times\mathbf{d}_3)+\gamma B_T(\hat{\mathbf{x}}\times\mathbf{d}_3)(\hat{\mathbf{x}}\times\mathbf{d}_3) - i\omega\sum_{j=1,2}(\mathbf{m}\times\hat{\mathbf{e}}_j)\hat{\mathbf{e}}_j, \tag{31}$$

where $B_T=(I/\gamma\hbar)(\lambda_T-\lambda)$. The difference in $\underline{\chi}(\omega)$, caused by $\lambda_T\neq\lambda$, is the emergence of a longitudinal resonance

$$\Omega_\parallel^2/\gamma^2=[p^2-(B_0/B_c)^2]B_T B_c \tag{32}$$

with the amplitude $\Lambda_\parallel^{zz}=1$; we obtain now $\Lambda_0^{zz}=0$ for the $\omega=0$ line. The $\Omega_\parallel$ resonance can be called an ''ordering-by-disorder'' peak since it originates directly from the fluctuations which stabilize the MF ground state having the largest entropy.

2. General field direction

For a single-**k** structure $\underline{\chi}(\omega)$ depends in the MF theory only on the directions of $\mathbf{B}_0$ and $\mathbf{Q}_j$ since $\mathbf{d}_j\|\mathbf{B}_0\times\mathbf{Q}_j$ and because the matrix $\underline{\Upsilon}(\omega)$ can be expressed using vectors which are proportional to $\mathbf{B}_0$, $\mathbf{Q}_j$ and $\mathbf{d}_j$. Therefore, in the appropriate coordinate system one can write $\underline{\chi}(\omega)$ using as a parameter only the angle θ between $\mathbf{B}_0$ and $\mathbf{Q}_j$. As before, this system can be defined as $\hat{\mathbf{z}}\|\mathbf{B}_0$ and $\hat{\mathbf{y}}\|\mathbf{B}_0\times\mathbf{Q}_j$ and $\hat{\mathbf{x}}=\hat{\mathbf{y}}\times\hat{\mathbf{z}}$. The explicit magnetic structure assuming $\mathbf{Q}_j=\mathbf{Q}_3$ is as follows:

$$\begin{aligned}&\mathbf{m}=(B_0/B_c)[\sin\theta(\cos\phi\hat{\mathbf{e}}_1+\sin\phi\hat{\mathbf{e}}_2)+\cos\theta\hat{\mathbf{e}}_3]\|\hat{\mathbf{z}},\\ &\mathbf{d}_1=\mathbf{d}_2=0,\\ &\mathbf{d}_3=[p^2-(B_0/B_c)^2]^{1/2}(\sin\phi\hat{\mathbf{e}}_1-\cos\phi\hat{\mathbf{e}}_2)\|\hat{\mathbf{y}}.\end{aligned} \tag{33}$$

One obtains two resonant frequencies Ω_+ and Ω_- given by

$$\Omega_\pm^2=\tfrac{1}{2}\{\omega_0^2+\gamma^2B_0^2\pm\sqrt{(\omega_0^2-\gamma^2B_0^2)^2+4\gamma^2B_0^2\omega_0^2\cos^2\theta}\}, \tag{34}$$

where $\omega_0^2=(B_D/B_c)\gamma^2(p^2B_c^2-B_0^2)$. The same result was first found[4] for antiferromagnetically ordered solid ^{3}He, and later for metallic fcc nuclear magnets.[15] A practical difference is that ω_0 has a strong field dependence in nuclear magnets but can be taken as a constant in solid ^{3}He. The amplitudes $\Lambda_\pm$ have not been given earlier; if we assume $\hat{\mathbf{y}}=\sin\phi\hat{\mathbf{e}}_1-\cos\phi\hat{\mathbf{e}}_2$ they can be written as

$$\Lambda_\pm^{xx}=\frac{\gamma^2B_0^2-\Omega_\mp^2}{\Omega_\pm^2-\Omega_\mp^2}+\frac{\Omega_+^2\Omega_-^2\cot^2\theta}{\gamma^2B_0^2(\Omega_\pm^2-\Omega_\mp^2)}, \tag{35a}$$

$$\Lambda_\pm^{yy}=\frac{\gamma^2B_0^2-\Omega_\mp^2}{\Omega_\pm^2-\Omega_\mp^2}, \tag{35b}$$

$$\Lambda_\pm^{zz}=\frac{\Omega_\mp^2(\Omega_\pm^2-\gamma^2B_0^2)}{\gamma^2B_0^2(\Omega_\pm^2-\Omega_\mp^2)}, \tag{35c}$$

$$\Lambda_\pm^{xy}=(\Lambda_\pm^{yx})^*=i\frac{\Omega_\pm(\gamma^2B_0^2-\Omega_\mp^2)}{\gamma B_0(\Omega_\pm^2-\Omega_\mp^2)}, \tag{35d}$$

$$\Lambda_\pm^{xz}=\Lambda_\pm^{zx}=-\frac{\Omega_+^2\Omega_-^2\cot\theta}{\gamma^2B_0^2(\Omega_\pm^2-\Omega_\mp^2)}, \tag{35e}$$

$$\Lambda_\pm^{yz}=(\Lambda_\pm^{zy})^*=i\frac{\Omega_\pm\Omega_\mp^2\cot\theta}{\gamma B_0(\Omega_\pm^2-\Omega_\mp^2)}. \tag{35f}$$

It can be seen that $\mathrm{Re}\{\underline{\Lambda}_-\}+\mathrm{Re}\{\underline{\Lambda}_+\}=\underline{I}$ which is consistent with the result $\underline{\chi}(0)=\chi_0\underline{I}$, obtained by using the static theory of Appendix I when $B\neq 0$ and $|\cos\theta|\neq 1$. The results of the dynamic and the static theory may disagree, however, when $\Omega_-\to 0$, as happens when $B_0\to 0$ or $|\cos\theta|\to 1$. In this case $\underline{\chi}(0)\neq\chi_0\underline{I}$ as was shown in Sec. III A 1. The discrepancy indicates that the dynamic theory does not necessarily yield the correct amplitude for the zero-frequency resonance when one of the nonzero resonant frequencies moves to zero. Instead, one must apply both theories to obtain $\underline{\chi}(\omega)$ in the limiting case as was done in Sec. III A 1.

The completely isotropic susceptibility of the single-**k** structure of Eq. (33) is in striking contrast with the zero-field behavior of the single-**k** configuration of Eq. (24), in which the susceptibility along the sublattice magnetization tends to zero with decreasing T.

B. Triple-k state

We assume $\mathbf{B}_0\|\hat{\mathbf{e}}_1+\hat{\mathbf{e}}_2$. In this case a triple-**k** structure seems favorable in large enough fields according to several calculations,[1,19] consistently with neutron-diffraction measurements on copper.[22] The state can be written as

$$\begin{aligned}&\mathbf{m}=(B_0/B_c)2^{-1/2}(\hat{\mathbf{e}}_1+\hat{\mathbf{e}}_2)\|\hat{\mathbf{z}},\\ &\mathbf{d}_1=\mathbf{d}_2=[(B_0/B_c)(p-B_0/B_c)]^{1/2}\hat{\mathbf{e}}_3\|\hat{\mathbf{y}},\\ &\mathbf{d}_3=(B_0/B_c-p)2^{-1/2}(\hat{\mathbf{e}}_1+\hat{\mathbf{e}}_2).\end{aligned} \tag{36}$$

If $B_0=0$, this reduces to a special case of Eq. (24); we assume $B_0>0$ from here on. Static susceptibility for this spin configuration is $\underline{\chi}(0)=\chi_0\underline{I}$ except for $B_0/pB_c=1/2$. Typically a small external field along $\hat{\mathbf{y}}$ twists $\mathbf{d}_1$ and $\mathbf{d}_2$ in the easy planes $\hat{\mathbf{e}}_1\cdot\mathbf{d}_1=0$ and $\hat{\mathbf{e}}_2\cdot\mathbf{d}_2=0$.

At $B_0/pB_c=1/2$, however, Eq. (36) assumes an exceptionally symmetric form with one half of the spins along

$\mathbf{B}_0$ and the other half parallel to $\hat{\mathbf{y}}$; in this case a field in the y direction turns $\mathbf{d}_3$ out of the easy-plane $\hat{\mathbf{e}}_3 \cdot \mathbf{d}_3 = 0$ and, for $p=1$, the susceptibility is reduced to $\chi_{yy}/\chi_0 = B_c/(B_c+B_D)$.

Therefore, the triple-**k** structure has generally a completely isotropic susceptibility, similarly to a single-**k** structure in an external field which is not in the direction of any of the crystalline axes. A structure which closely resembles Eq. (36) can also be found when $\mathbf{B}_0$ is along a crystal axis.[19] Its properties are, however, more complicated because the spin configuration is somewhat less symmetric than predicted by Eq. (36). We do not discuss this case in more detail.

For the configuration given by Eq. (36), there are two resonances with $\omega \neq 0$, one in the component parallel to the static field and the other in the transverse components of the susceptibility matrix. The transverse resonant frequency $\omega = \Omega_\perp$ is given by

$$\Omega_\perp^2/\gamma^2 = B_0^2 + B_D(pB_c - B_0)p \ . \tag{37}$$

The nonzero components of the amplitude $\underline{\Lambda}_\perp$ at the resonance are

$$\Lambda_\perp^{xx} = 1, \quad \Lambda_\perp^{xy} = (\Lambda_\perp^{yx})^* = i\gamma B_0/\Omega_\perp, \quad \Lambda_\perp^{yy} = (\gamma B_0/\Omega_\perp)^2. \tag{38}$$

Apart from the value of the resonant frequency, $\underline{\Lambda}_\perp$ is thus of the same form as Eq. (28). For the parallel resonance at $\omega = \Omega_\parallel$ we find

$$\Omega_\parallel^2/\gamma^2 = (B_D/B_c)B_0(pB_c - B_0) \tag{39}$$

and $\Lambda_\parallel^{zz} = 1$.

At $\Omega = 0$ there is a transverse resonance with

$$\Lambda_0^{yy} = \chi_{yy}/\chi_0 - (\gamma B_0/\Omega_\perp)^2, \tag{40}$$

where $\chi_{yy} = \chi_0$ except at $B_0/pB_c = 1/2$ as discussed above.

IV. SIMULATION STUDIES OF SPIN DYNAMICS

Thermal fluctuations lead to deviations from the mean-field theory outlined above. Their origin is the inaccuracy of the MF assumption $\langle I_i^\mu I_j^\nu \rangle = \langle I_i^\mu \rangle \langle I_j^\nu \rangle$. To study these effects we investigate by direct numerical simulation classical spins interacting through the Hamiltonian

$$\mathcal{H} = J_1 \sum_{i>j}^{\mathrm{NN}} \hat{\mathbf{S}}_i \cdot \hat{\mathbf{S}}_j + D_1 \sum_{i>j}^{\mathrm{NN}} \hat{\mathbf{S}}_i \cdot [\underline{I} - 3\hat{\mathbf{r}}_{ij}\hat{\mathbf{r}}_{ij}] \cdot \hat{\mathbf{S}}_j + J_2 \sum_{i>j}^{\mathrm{NN}} \hat{\mathbf{S}}_i \cdot \hat{\mathbf{S}}_j - \mathbf{B} \cdot \sum_i \hat{\mathbf{S}}_i, \tag{41}$$

where $\hat{\mathbf{S}}_i$'s indicate the N spin vectors at the fcc lattice sites. We have replaced $(\gamma\hbar/I)\mathbf{B}$ in Eq. (1) by $\mathbf{B}$. Both the Hamiltonian of Eq. (1) and the temperature of the quantum-spin model have been divided by I^2 and the classical limit $I \to \infty$ has been taken to obtain the Hamiltonian of Eq. (41) and the corresponding classical temperature. We measure the magnetic field $\mathbf{B}$ and the angular frequency ω in terms of the energy J_1 and give $\chi^{\alpha\beta}$ as $N^{-1}\Sigma_i \partial\langle S_i^\alpha \rangle/\partial B^\beta$, i.e., using the units[23] of the inverse energy J_1^{-1}.

In order to stabilize type-I order we select $J_1 > 0$, $J_2 = -0.15J_1$ and $D_1 = 0.35J_1$; in this case the global minimum of the eigenvalues of $\underline{A}(\mathbf{q})$ occurs for type-I ordering vectors.[24] D_1 corresponds to a moderately large anisotropy, about the same magnitude as was found for the nearest-neighbor silver nuclei.[25] We obtain the eigenvalues $\lambda = -4(J_1 + D_1) + 6J_2$, $\lambda_1 - \lambda = 12D_1$, and $\lambda_0 = 12J_1 + 6J_2$ for the spin-spin interactions of the model given by Eq. (41).

A. Monte Carlo studies of ground-state selection

We study a lattice of $N = 16^3 = 4096$ spins with periodic boundary conditions, using the MC algorithm[26] of Ref. 27. Before discussing dynamical considerations in Secs. IV B–IV D we describe briefly how we deduce the stability of the structures that were investigated in Sec. III for the static case.

In zero field, we inferred from slow cooling and heating runs that the spins undergo a transition between paramagnetic and type-I states at $k_B T_N/J_1 = 1.07 \pm 0.02$. We found, therefore, a reduction of $T_N^{\mathrm{MF}}/T_N^{\mathrm{MC}} \approx 2.0$ from the MF value. The spin configuration is the state given by Eq. (24), with $\hat{\mathbf{y}}$ along a crystal axis. We systematically found this structure also after abrupt quenches from $T = \infty$ to $T/T_{\mathrm{N}} \approx 0.2$. Altogether 10 quenches were carried out by starting from a random spin structure[26] and by simulating 2000 Monte Carlo updates per spin (MCS) at $k_B T/J_1 = 0.2$. We found $|\mathbf{d}_j| \approx 0.94$ and 9 times $\mathbf{d}_j$ was along a crystal axis perpendicular to $\mathbf{Q}_j$ within 7° at the end of the simulation. Once we found an angle of 16° which appeared to result form a slow decay of a structure with an angle of about 45° between $\mathbf{d}_j$ and the crystal axes in the easy-plane $\mathbf{d}_j \cdot \hat{\mathbf{e}}_j = 0$.

The collinearity of the zero-field structure is consistent with Monte Carlo simulations of models with only isotropic nearest-neighbor interactions.[28–30] As a consequence of the dipolar interaction, spins align parallel to a crystalline axis.[27,31,32] According to some calculations, however, spins should have an angle of 45° with a crystalline axis.[19]

In external fields, there are several possibilities for the angle between $\mathbf{B}$ and $\mathbf{Q}_j$: the difference in their free energies vanish when $B \to 0$. There is also the possibility for triple-**k** structures. As a result, metastable states might appear in quenches and a careful procedure must be used to determine the ground state.

We carried out five cooling runs[26] at $B/B_c = 0.2$ with $\mathbf{B} \| \hat{\mathbf{e}}_3$. The simulations were started from a random spin configuration at $k_B T/J_1 = 1.2$, and T was reduced in 10 steps to $k_B T/J_1 = 0.9$. At each temperature, 2000 Monte Carlo updates per spin (MCS) were carried out. In all runs the configuration given by Eq. (24) was found below the ordering temperature, with either $\mathbf{d}_3 \| \hat{\mathbf{e}}_1$ or $\mathbf{d}_3 \| \hat{\mathbf{e}}_2$ within the statistical accuracy.

We also studied the field direction $\mathbf{B} \| \hat{\mathbf{e}}_2 + \hat{\mathbf{e}}_3$ with $B/B_c = 0.2$. A similar cooling procedure was employed as described above for $\mathbf{B} \| \hat{\mathbf{e}}_3$. In all five simulations, we found the configuration

$$\begin{aligned} &\mathbf{m} = (B_0/B_c)(\hat{\mathbf{e}}_1 + \hat{\mathbf{e}}_2) \| \hat{\mathbf{z}}, \\ &\mathbf{d}_1 = \mathbf{d}_3 = 0, \\ &\mathbf{d}_2 = [p^2 - (B_0/B_c)^2]^{1/2} \hat{\mathbf{e}}_3 \| \hat{\mathbf{y}}, \end{aligned} \tag{42}$$

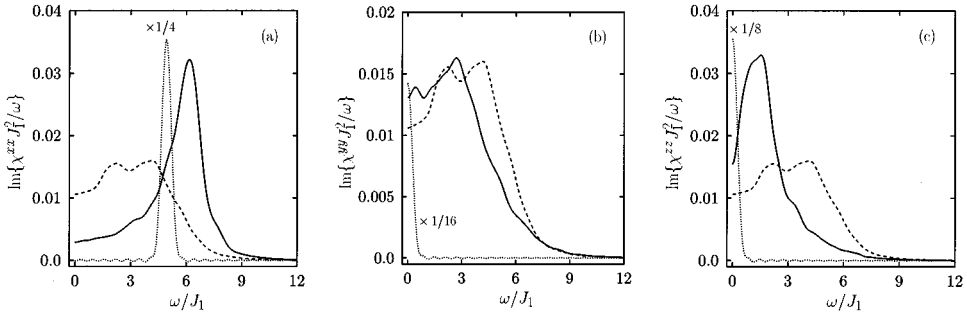

FIG. 2. (a)–(c): Form functions for magnetic resonance in zero external field as given by simulations of spin dynamics: Dashed lines have been calculated for $k_BT/J_1=1.15$ above the antiferromagnetic ordering temperature, while the continuous curves are for $k_BT/J_1=1.0$ below T_N. The AF spin structure is given by Eq. (24) with $p=0.58$ and $\hat{\mathbf{y}}=\hat{\mathbf{e}}_2$. Dotted lines correspond to mean-field results. In (a), (b), and (c) the MF spectra have been divided by 4, 16, and 8, respectively, to fit them into the figures.

or a structure with $\mathbf{d}_1\|\hat{\mathbf{e}}_3$ and $\mathbf{d}_2=\mathbf{0}$; the configurations are related by a symmetry operation. The structure in Eq. (42) is equivalent to Eq. (33) when $\theta=\pi/4$.

As a third case, we investigated $\mathbf{B}\|\hat{\mathbf{e}}_2+\hat{\mathbf{e}}_3$ with $B/B_c=0.4$. In all five runs we found the triple-**k** structure of Eq. (36) with various sign combinations of $\mathbf{d}_j$, resulting from different selections for the origin of the space coordinate $\mathbf{r}_i$ in Eq. (2).

Our results for the ground-state selection, both for the single-**k** and triple-**k** structures, are in good agreement with earlier Monte Carlo simulations which were used to model the spin system of silver.[31,32]

B. Dynamics: Numerical techniques

Our numerical scheme to obtain NMR spectra is in many ways similar to our earlier approach,[14] which dealt with the NMR response of exchange-coupled spin systems of two spin species in a high external magnetic field. Our method is also similar to the techniques employed in the calculation of the dynamic structure factor.[34,35] Linear-response theory[36] yields the dynamic susceptibility

$$\underline{\chi}(\omega)=\frac{1}{k_BT}[\underline{C}(t=0)+i\omega\underline{C}(\omega)], \tag{43}$$

where $\underline{C}(\omega)=\int_0^\infty\underline{C}(t)e^{i\omega t}dt$. The autocorrelation matrix $\underline{C}(t)$ is given by

$$\underline{C}(t)=\frac{1}{N}\langle[\mathbf{M}(t_0+t)-\langle\mathbf{M}\rangle][\mathbf{M}(t_0)-\langle\mathbf{M}\rangle]\rangle. \tag{44}$$

Here $\mathbf{M}=\Sigma_i\hat{\mathbf{S}}_i$ is the total spin. $\underline{C}(t)$ was evaluated for a state reached by simulated cooling.

The time dependence of **M** was found by solving the microscopic equations of motion

$$\frac{d\hat{\mathbf{S}}_i}{dt}=\frac{\partial\mathcal{H}}{\partial\hat{\mathbf{S}}_i}\times\hat{\mathbf{S}}_i. \tag{45}$$

The conventional fourth-order Runge-Kutta method, with the time step $\Delta t=0.04J_1^{-1}$, was employed to solve Eqs. (45). During integrations, lengths of spins were conserved within 0.001 and internal energy per spin within $0.001J_1$.

Fourier transforms of autocorrelations were calculated from

$$\underline{C}(\omega)=\int_0^{t_{\max}}\underline{C}(\tau)\exp[-(\tau\sigma)^2/2+i\omega\tau]d\tau. \tag{46}$$

We selected $t_{\max}$ by setting $\exp[-(t_{\max}\sigma)^2/2]=0.05$ so that the finite-time cutoff produced only weak spurious oscillations. This scheme convolves $\underline{C}(\omega)$ with a resolution distribution which is approximately $(\sqrt{2\pi}\sigma)^{-1}\exp(-\omega^2/2\sigma^2)$. An average over n integrations from different initial conditions was taken in evaluating the autocorrelation matrix, Eq. (45). We employed $\sigma/J_1=0.25$ and $n=200$. The t_0 average was calculated over $0.5t_{\max}$; the total evolution time for each initial state was, therefore, $1.5t_{\max}$ after which a simulation of 200 MC updates per spin was carried out to produce the initial state for the next time integration.[37] The average value of $\langle\mathbf{M}\rangle$ was used during the total time of all integrations.

To compare the MF results with the direct numerical procedure we calculated the autocorrelation matrix within the MF theory. $\underline{C}^{\mathrm{MF}}(t)$ was then transformed to $\underline{\chi}(\omega)$ in the same way as $\underline{C}(t)$. This procedure replaced the δ functions in the anti-Hermitian part of $\underline{\chi}^{\mathrm{MF}}(\omega)$ by similar resolution distributions as were used in the spin dynamics simulation.

C. Dynamics in zero field

In Figs. 2(a)–2(c) the dashed lines indicate the paramagnetic spectrum at $T/T_N^{\mathrm{MC}}=1.07$ in zero external magnetic field. The curves were calculated under the assumption of direction independence: $\underline{\chi}(\omega)=\mathrm{Tr}\{\underline{\chi}(\omega)\}I/3$. This holds within our numerical accuracy. The static susceptibility is about 95% of the MF-predicted χ_0 for the ordered state.

All continuous curves in Figs. 2(a)–2(c) are spectra for the single-**k** structure of Eq. (24) at $T/T_N^{\mathrm{MC}}=0.93$. The sublattice polarization is $\langle p\rangle_{\mathrm{MC}}\approx0.58$, as calculated from

$$|\mathbf{m}|^2+|\mathbf{d}_1|^2+|\mathbf{d}_2|^2+|\mathbf{d}_3|^2=p^2, \tag{47}$$

with an average over the simulations [see Eq. (2)]. The main resonance, Eq. (27), can be seen in Fig. 2(a). The ''ordering-by-disorder'' peak, Eq. (32), is displayed in Fig. 2(c). This peak can be analyzed for the strength of the effective thermal

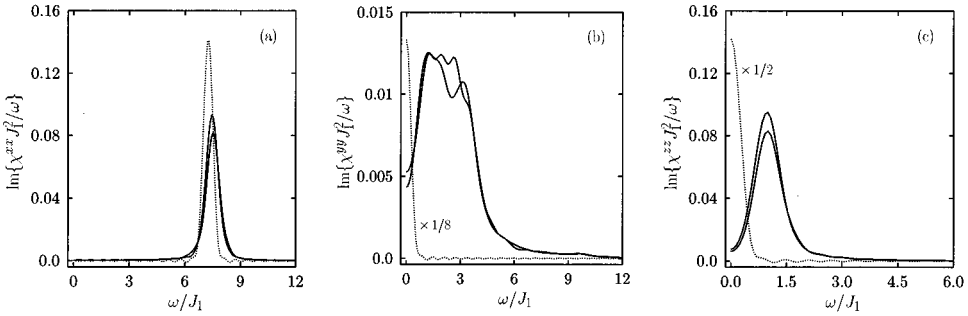

FIG. 3. (a)–(c): Form functions when $B=0$ and $k_BT/J_1=0.5$. The spin structure is given by Eq. (24) with $p=0.85$ and $\hat{\mathbf{y}}=\hat{\mathbf{e}}_2$. Continuous lines are spectra obtained from simulations and dotted lines correspond to MF results. Results of two simulations are shown to illustrate the numerical accuracy. In (b) and (c) the MF spectra have been divided by 8 and 2, respectively.

anisotropy: we obtain $B_T/B_D=(\Omega^{zz}_{\rm MC}/\Omega^{xx}_{\rm MC})^2=0.03\cdots0.06$. The errors are rather large since the peak is not very sharp.

Both in Fig. 2(a) and in Fig. 2(c) the integrated static susceptibility agrees within 2% with the MF result χ_0, although we believe that the accuracy of our simulated $\chi(0)$ is only about 10%. In Fig. 2(b), the shape of $\mathrm{Im}\{\overline{\chi}^{yy}/\omega\}$, which corresponds to the component parallel to the antiferromagnetic moment $\mathbf{d}_3\|\hat{\mathbf{e}}_2\|\hat{\mathbf{y}}$, is very similar to the paramagnetic spectrum shown by the dashed curve. The static susceptibility seems to agree with $\chi^{yy}/\chi_0=0.80$, obtained from the MF Eq. (26) using $p=\langle p\rangle_{\rm MC}=0.58$. At lower temperatures, however, the agreement becomes worse. At $T/T_N^{\rm MC}=0.48$, see Fig. 3(b), we found that Eq. (26) with $p=\langle p\rangle_{\rm MC}$ yields a susceptibility which is about 25% smaller than the value found from simulations. At $T/T_{\rm N}^{\rm MC}=0.24$ the MF prediction is 40% smaller than the simulated result. Better agreement could probably be obtained by calculating $\chi(0)$ using a more realistic approach like the spin-wave theory.[38]

It is interesting to compare the peak positions $\Omega^{xx}_{\rm MC}$ of the simulated $\mathrm{Im}\{\chi^{xx}/\omega\}$ curves with MF predictions. There are two ways to do this. The MF resonant frequencies can be calculated either by using $p_{\rm MF}$ at real temperatures for sublattice polarizations p, or by taking $p=\langle p\rangle_{\rm MC}$. We find that $\Omega^{xx}_{\rm MC}$ is estimated better by using $\langle p\rangle_{\rm MC}$ at large polarizations, whereas when T is only slightly less than $T_N^{\rm MC}$ use of $p=p_{\rm MF}$ yields a more accurate result. However, the form-function-averaged resonant frequency, $\int_0^\infty \mathrm{Im}\{\chi^{xx}\}d\omega/\int_0^\infty \mathrm{Im}\{\chi^{xx}/\omega\}d\omega$ is in each case estimated better by $\langle p\rangle_{\rm MC}$. In the figures, we always calculate the MF curves using $p=\langle p\rangle_{\rm MC}$.

In Figs. 3(a)–3(c) we have evaluated the spectra for the configuration of Eq. (24) at the temperature $T/T_N^{\rm MC}=0.48$ where $\langle p\rangle_{\rm MC}\approx0.85$. The agreement between the MF theory, using $p=\langle p\rangle_{\rm MC}$, and the simulation is now considerably better for the main peak, as is found by comparing Fig. 3(a) with Fig. 2(a). The peak due to thermal anisotropy, shown in Fig. 3(c), is clearly sharper than at $T/T_N^{\rm MC}=0.93$. For the anisotropy field we obtain $B_T/B_{\rm D}=(\Omega^{zz}_{\rm MC}/\Omega^{xx}_{\rm MC})^2=0.018$. In a run at $T/T_N^{\rm MC}=0.24$ we found $B_T/B_D=0.011$. The integrated intensities of the MF and simulated peaks agree within statistical accuracy in Figs. 3(a) and 3(c), while the situation is worse in Fig. 3(b) as discussed earlier.

D. Dynamics in external fields

*1. Single-***k** *structures*

The continuous line in Figs. 4(a)–4(c)is the spectrum of the single- **k** structure of Eq. (24) at $\mathbf{B}/B_c=0.2\hat{\mathbf{e}}_3$, when $T/T_N^{\rm MC}=0.48$; this corresponds to $\langle p\rangle_{\rm MC}\approx0.85$. The relation $\langle\mathbf{m}\rangle=\mathbf{B}/B_c$ was found to be valid for the MC simulations in the ordered state within about 1%. Because of the external field, the primary antiferromagnetic resonance can be seen also in the diagonal component for the direction parallel to the antiferromagnetic moment $\mathbf{d}_3$, as is shown by Fig. 4(b). The canting caused by **B** makes Eq. (26) somewhat more accurate, and the MF result for static χ^{yy} is now only 15% smaller than in the simulation. The discrepancy can be attrib-

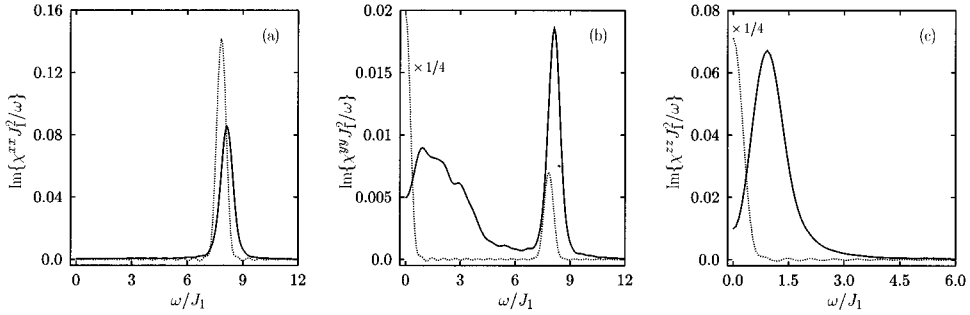

FIG. 4. (a)–(c): Form functions at $B/B_c=0.2$ when $\mathbf{B}\|\hat{\mathbf{e}}_3$ and $k_BT/J_1=0.5$. Polarization $p=0.85$ and the spin structure is given by Eq. (24) with $\hat{\mathbf{y}}=\hat{\mathbf{e}}_2$. Continuous lines: simulations; dotted lines: MF results. In (b) and (c) the MF spectra have been divided by 4.

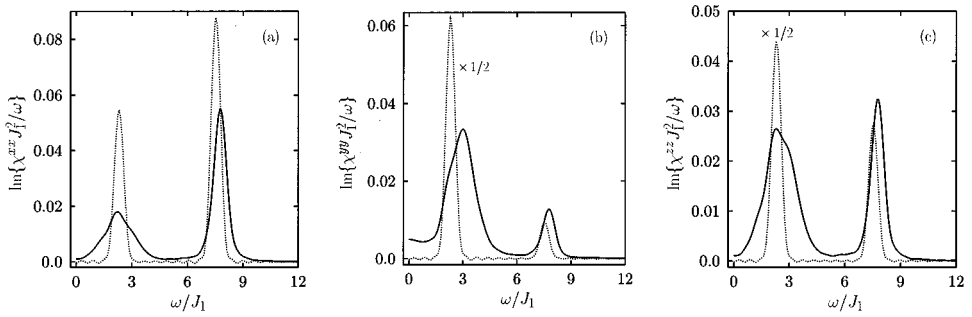

FIG. 5. (a)–(c): Form functions at $B/B_c=0.2$ when $\mathbf{B}\|\hat{\mathbf{e}}_1+\hat{\mathbf{e}}_2$ and $k_BT/J_1=0.5$. Polarization $p=0.85$ and the spin structure is given by Eq. (42). Continuous lines: simulations; dotted lines: MF results of Sec. III A 2. In (b) and (c) the MF spectrum has been divided by 2.

uted to low-frequency contributions $\omega/J_1<6$, while the intensity of the resonance peak at $\omega/J_1\approx 8.1$ is in close agreement with the MF formula, Eq. (28), using $p=\langle p\rangle_{\mathrm{MC}}$. The intensities of the simulated peaks and MF resonances in Figs. 4(a) and 4(c) agree within numerical accuracy. We found for $B_T/B_D=0.015$ by solving Eqs. (27) and (32).

Our results for the single-**k** structure of Eq. (42) in a field $\mathbf{B}\|\hat{\mathbf{e}}_1+\hat{\mathbf{e}}_2$ are shown in Figs. 5(a)–5(c) when $B/B_c=0.2$ and $T/T_N^{\mathrm{MC}}=0.48$. The sublattice polarization is again $\langle p\rangle_{\mathrm{MC}}\approx 0.85$. The MF dynamics of this structure is discussed in Sec. III A 2. The intensities of the simulated peaks and the MF resonances are in agreement, except for the case illustrated in Fig. 5(b) where the intensity of the simulated low-frequency peak is 12% smaller than the MF prediction. The low-frequency peaks are rather wide and have an interesting shape; there is some intensity even at zero-frequency as is seen from Fig. 5(b).

*2. Triple-***k** *structure*

Spectra for the triple-**k** structure of Eq. (36) in a field $\mathbf{B}\|\hat{\mathbf{e}}_1+\hat{\mathbf{e}}_2$ are shown in Figs. 6(a)–(c). The simulation was carried out at $B/B_c=0.4$ and $T/T_N^{\mathrm{MC}}=0.48$ where $\langle p\rangle_{\mathrm{MC}}\approx 0.85$. The perpendicular resonances can be seen in Figs. 6(a) and 6(b). The $\omega=0$ peak, predicted by the MF theory [see Eq. (40)], has shifted to a finite frequency in the simulation as is shown by Fig. 6(b). The static susceptibilities obtained from the simulations are smaller by 15 and 25 % than the MF results in Figs. 6(a) and 6(b), respectively. The discrepancy for intensity is particularly large for the low-frequency peak in Fig. 6(b). These effects might be caused by an effective thermal anisotropy which was considered in detail for a single-**k** configuration in Sec. III A 1. The susceptibility anomaly at $B/B_c=p/2=0.425$, discussed in Sec. III B, might also play a role. However, for the parallel peak shown in Fig. 6(c), the simulated intensities are in close agreement with the MF result.

When we studied the spin dynamics in a slightly higher field, $B/B_c=0.5$, but at the same temperature, an interesting qualitative difference was found: The low-frequency peak in $\mathrm{Im}\{\chi^{yy}(\omega)\}/\omega$ then is at $\omega=0$, indicating the presence of an AF soft mode which is not destroyed by thermal anisotropy.

V. COMPARISON WITH EXPERIMENTS

NMR measurements have been made on the antiferromagnetically ordered states of copper and silver.[39–41] The experiments were done on polycrystalline foils by employing the continuous-wave technique. Since the direction of the external magnetic field with respect to the crystalline axes affects the spin structure and hence the NMR line shape as well, it is rather difficult to analyze the data in detail when the field is different from zero.

A. Copper

We have compared the simulated and measured[39] NMR spectra of copper in our earlier paper.[6] Experiments in zero field revealed two resonances in the NMR absorption curve. The one at high frequencies was interpreted as the conventional AF resonance, while the one at low frequencies was identified as the ''ordering-by-disorder'' peak of a single- **k** structure [see Fig. 2(c)]. A rather good fit between the measured and simulated results was found by assuming that the experimental data correspond to a superposition of antiferromagnetic and paramagnetic domains.

B. Silver

Hakonen and his co-workers have measured NMR line shapes of antiferromagnetically ordered silver nuclei in a polycrystalline sample below T_N = 560 pK.[40,41] The spectra were characterized by two antiferromagnetic resonant fre-

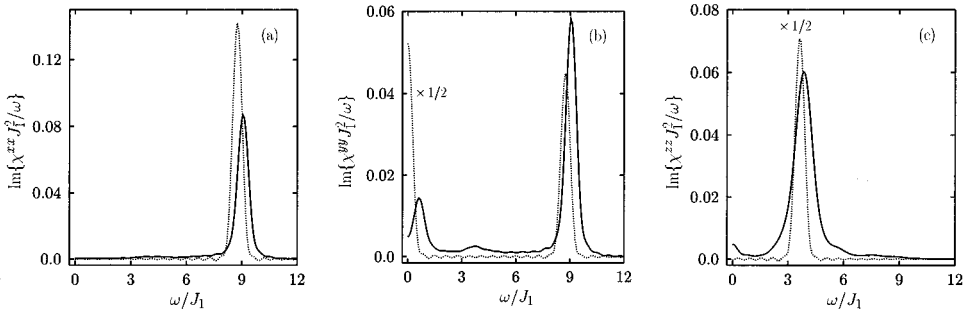

FIG. 6. (a)–(c): Form functions at $B/B_c=0.4$ when $\mathbf{B}\|\hat{\mathbf{e}}_1+\hat{\mathbf{e}}_2$ and $k_BT/J_1=0.5$. Polarization $p=0.85$ and the spin structure is the triple-**k** configuration of Eq. (36). Continuous lines: simulations; dotted lines: MF results. In (b) and (c) the MF spectrum has been divided by 2.

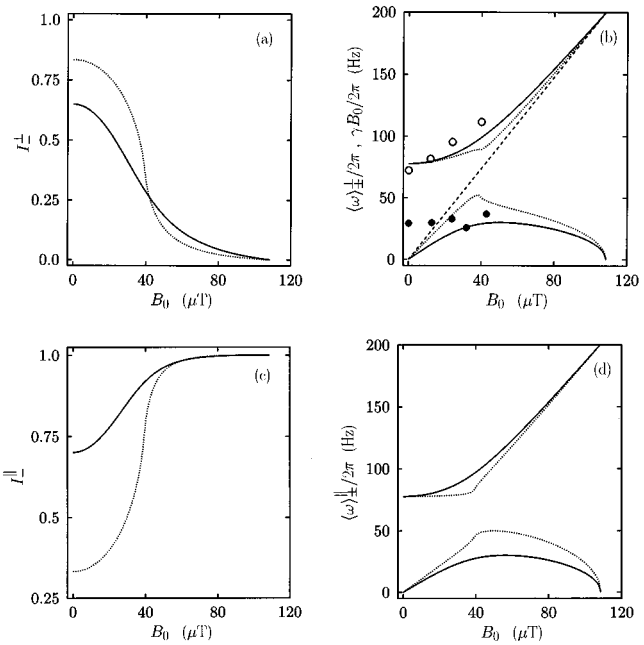

FIG. 7. Calculated intensities and positions of antiferromagnetic resonances in silver for an axial excitation field transverse ($\perp$) or parallel ($\parallel$) to the static external field. A single-**k** structure with polarization $p=0.7$ is assumed. (a,c) Intensity of the lower absorption band for transverse and parallel excitations, respectively. (b,d) Average frequencies of the lower and upper resonances for transverse and parallel excitations. The dashed line in (b) shows the Larmor frequency $\gamma B_0/2\pi$ of isolated spins for comparison. Solid and open circles in (b) indicate the measured positions of the lower and upper modes, respectively (Ref. 40 and 41). In all frames the continuous lines correspond to the case in which the ordering vector maximizing $(\mathbf{B}_0\cdot\mathbf{Q}_j)^2$ is selected in each microcrystallite; the dotted curves show the result for an equal distribution of the three type-I ordering vectors.

quencies. The observed positions of the resonances have been indicated in Fig. 7(b) at different external magnetic fields.

According to recent neutron-diffraction measurements,[2] the ordered spin structure of silver is a single-**k** type-I state when $\mathbf{B}_0\parallel[001]$. The spin configuration for other field alignments has not been investigated by neutrons so far. According to theoretical calculations,[19,31–33] triple-**k** structures should be stable in elevated fields. However, for various field directions with $B_0<30$ μT, single-**k** states should dominate the phase diagram. Therefore, we try to interpret the data on this basis.

The dynamic susceptibility matrix of a single-**k** structure in an external field was given in Sec. III A 2. In polycrystals, the resonant frequencies of Eq. (34) form two bands, $|\omega|\leqslant\min\{\gamma B_0,\omega_0\}$ and $\max\{\gamma B_0,\omega_0\}\leqslant|\omega|\leqslant\sqrt{\gamma^2B_0^2+\omega_0^2}$. We calculate the absorption spectra for these two cases.

(i) We first assume that fluctuations stabilize, among the three possibilities, the single-**k** structure for which the ordering vector maximizes $(\mathbf{Q}_j\cdot\mathbf{B}_0)^2$. The condition of maximum $(\mathbf{Q}_j\cdot\mathbf{B}_0)^2$ is the simplest possible selection rule which is consistent with the neutron-diffraction data[2] and with most of the theoretical predictions,[19,31–33] including the low-field MC simulations of Sec. IV.

When ω is in one of the two bands and $\omega>0$ the dissipative part of $\underline{\chi}(\omega)$ becomes

$$\underline{\chi}_{\mathrm{AH}}(\omega)/\omega=\frac{3\pi i\chi_0}{2}\Pi(\cos\theta)\underline{\tilde{\Lambda}}_{\pm}\left|\frac{\partial\Omega_{\pm}}{\partial\cos\theta}\right|^{-1}_{\omega^2=\Omega_{\pm}^2(\cos\theta)}, \tag{48}$$

where the subscript AH denotes the anti-Hermitian part of $\chi(\omega)$. The quantity $\cos\theta$ is the positive root of the equation $\bar{\Omega}_{\pm}^2(\cos\theta)=\omega^2$, and subscripts + and − denote the upper and the lower bands, respectively. For $\omega<0$, the matrix $\underline{\tilde{\Lambda}}_{\pm}$ in Eq. (48) should be replaced by its complex conjugate. The quantity $\Pi(\cos\theta)$ is just the probability with which the angle $\theta<\pi/2$ between $\mathbf{B}_0$ and a crystalline axis is the smallest of the three possibilities when all orientations of the crystallites have the same probability. We find

$$\Pi(\cos\theta)=\begin{cases}1, & \cos\theta\geqslant1/\sqrt{2}\\ 1-(4/\pi)\operatorname{arccoscot}\theta, & 1/\sqrt{3}<\cos\theta<1/\sqrt{2}.\\ 0, & \cos\theta\leqslant1/\sqrt{3}\end{cases} \tag{49}$$

The nonzero components of the matrix $\underline{\tilde{\Lambda}}_{\pm}$ are

$$\tilde{\Lambda}^{xx}_{\pm}=\tilde{\Lambda}^{yy}_{\pm}=(\Lambda^{xx}_{\pm}+\Lambda^{yy}_{\pm})/2,\quad \tilde{\Lambda}^{xy}_{\pm}=(\tilde{\Lambda}^{yx}_{\pm})^*=\Lambda^{xy}_{\pm},$$
$$\tilde{\Lambda}^{zz}_{\pm}=\Lambda^{zz}_{\pm}. \tag{50}$$

The quantities on the right-hand sides were given by Eq. (35).

Equation (48) can be obtained as follows: $\chi_{\mathrm{AH}}(\omega)$ is first averaged over orientations of microcrystallites using Eq. (19) and Eqs. (34) and (35). The orientations can be parametrized by three Euler angles. The first fixes the $\hat{\mathbf{y}}$ axis in Eq. (33) with respect to the laboratory coordinates; in the calculation $\underline{\Lambda}_{\pm}$ is replaced with its average $\underline{\tilde{\Lambda}}_{\pm}$ over all rotations about $\hat{\mathbf{z}}$. The quantity θ can be selected as the second Euler angle. In the course of the calculation one can employ the formula

$$g(\omega)=\int_0^{\pi/2}f(\cos\theta)\,\delta[\omega-\Omega_{\pm}(\cos\theta)]\sin\theta\,d\theta$$
$$=f(\cos\theta)\left|\frac{\partial\Omega_{\pm}(\cos\theta)}{\partial\cos\theta}\right|^{-1}_{\omega=\Omega_{\pm}(\cos\theta)}. \tag{51}$$

The average over the third angle, related to ϕ in Eq. (33), yields the function $\Pi(\cos\theta)$.

(ii) In the second case there is no preference between the three type-I ordering vectors in various crystallites and all values $\cos\theta$ are equally probable. The spectrum for positive frequencies is then simply

$$\underline{\chi}_{\mathrm{AH}}(\omega)/\omega=\frac{\pi i\chi_0}{2}\underline{\tilde{\Lambda}}_{\pm}\left|\frac{\partial\Omega_{\pm}}{\partial\cos\theta}\right|^{-1}_{\omega^2=\Omega_{\pm}^2(\cos\theta)}, \tag{52}$$

where the notations are the same as in Eq. (48).

The resonant frequencies, which are obtained from Eqs. (52) and (52), are restricted to two bands which can be rather sharp. Some components of Eq. (52) even have integrable singularities of the type $1/\sqrt{|\Omega_0-\omega|}$ at the top of the lower or at the bottom of the higher band which occur at $\Omega_0=\gamma B_0$ or at $\Omega_0=\omega_0$.

It is of interest to study the intensities $I_\pm$ of the two bands, defined by $I_\pm^\perp=(2/i\pi\chi_0)\int_\pm \chi_{\rm AH}^{xx}(\omega)d\omega/\omega$ or $I_\pm^\parallel=(2/i\pi\chi_0)\int_\pm \chi_{\rm AH}^{zz}(\omega)d\omega/\omega$, where $\int_\pm d\omega$ indicates integration over a positive-frequency band. The sums of the intensities satisfy $I_-^\perp+I_+^\perp=I_-^\parallel+I_+^\parallel=1$. Figure 7 illustrates results for the case $p=0.7$ with exchange parameters such that $B_c=155$ μT and $B_D/B_c=0.15$, which correspond to the calculated forces between nuclear spins in silver.[25,42]

Figure 7(a) shows $I_-^\perp$, the intensity of the low-frequency branch of the spectrum when the excitation field is transverse to the external field, as a function of B_0. Since $I_+^\perp=1-I_-^\perp$, the ratio $I_-^\perp/I_+^\perp$ decreases with field as observed.[43] The decrease is considerably smaller when the ordering vectors maximizing $(\mathbf{B}_0\cdot\mathbf{Q}_j)^2$ are selected than when all domains are equally populated. Important additional insight to the domain selection can be obtained by measuring also the parallel resonance, shown in Fig. 7(c), since the difference between the two domain distributions is then larger.

Average frequencies of the upper and lower bands are given by $\langle\omega\rangle_\pm^\perp=(2/i\pi\chi_0 I_\pm^\perp)\int_\pm \chi_{\rm AH}^{xx}(\omega)d\omega$ and $\langle\omega\rangle_\pm^\parallel=(2/i\pi\chi_0 I_\pm^\parallel)\int_\pm \chi_{\rm AH}^{zz}(\omega)d\omega$; these quantities are shown in Figs. 7(b) and 7(d) for the transverse and parallel resonances, respectively. In the transverse case, it is possible to compare our calculations against the NMR measurements of Hakonen *et al.*[40,41] There is rather good agreement. It seems, therefore, that the observed resonances can be interpreted in terms of a single magnetically ordered phase with a single-**k** structure. The same conclusion was made by the experimentalists.[40,41] One has to note, however, that the experimental positions of the high- and low-frequency branches were obtained using a rather complicated procedure. It is not clear how a rigorous comparison should be carried out; the problem is especially difficult for the low-frequency mode.

Finally we would like to remark that the ground-state configuration of a single-**k** state is a subtle problem in low external fields, when $\mathbf{B}_0$ is not perpendicular to any of the crystalline axes. The reason is the conflict between fluctuation-induced thermal anisotropy and Zeeman energy. As we found in our Monte Carlo simulations, discussed in Sec. IV A, spins at zero field align along a crystalline axes, and so does the corresponding $\mathbf{d}_j$ vector. In a field, however, MF theory requires $\mathbf{d}_j\|\mathbf{B}_0\times\mathbf{Q}_j$ [see Eq. (33)]. Therefore, for most field directions, a significant reorientation of spins should occur in low fields. The nature of this transition is not known. One can expect that, at least in some field directions, the reorientation is similar to a spin-flop transition.[8] It is of first order and can, therefore, show hysteresis. The spin-flop field should be on the order of $\sqrt{B_T B_c}$ which, for the fluctuations fields found in Sec. IV C, is somewhat below $0.1B_c$. More experimental and theoretical work is needed to understand this reorientation process in silver.

VI. CONCLUDING REMARKS

We extended earlier MF calculations[15] to extract NMR spectra for type-I antiferromagnets. MF predictions were compared with results obtained using numerical methods. Our computational technique combines Monte Carlo simulations with numerical solutions of the equations of motion. This makes it possible to calculate complete NMR absorption line shapes for a classical spin system including dipolar interactions with neighboring spins. One has to remember, however, that our technique is practical only for spin Hamiltonians with short range spin-spin interactions. Simulations of such models enabled us to compare the locations and intensities of the mean-field NMR resonances against in-principle-exact numerical results. Although the dipole-dipole interaction was truncated to nearest neighbors, with a strength of the same magnitude as between nuclear spins in silver, the results are expected to be qualitatively similar for a large range of interaction constants. Apart from the type-I ground state, the only essential assumption we made was the sign of the anisotropic spin-spin interaction.

The simulations sorted out the cases where the MF approach is adequate from those where it fails to describe the essential dynamics. Simulations provide probably the most powerful practical method to calculate NMR spectra for disordered spin structures in paramagnetic regions. Slightly above the ordering temperature, the spectra can show nontrivial precursor effects caused by short-range correlations.

In the ordered states the MF theory proved useful. We found, for example, that the MF prediction for the principal AF resonance, in the direction perpendicular to the magnetic moments, is rather good. However, the MF theory fails almost completely in its description of the diagonal component of the dynamic susceptibility tensor along the direction parallel to the antiferromagnetic moments: In these cases the extended low-frequency intensity distributions in χ/ω cannot be accounted for by the MF theory.

We found that in some cases thermal effects which lift the degeneracy of the mean-field ground states can be seen directly by inspecting a suitable component of the dynamic susceptibility matrix. We modeled the removal of the MF degeneracy by introducing an effective thermal anisotropy field and studied its strength numerically. At $T\approx T_N$, the thermal anisotropy field, which confines the spins to the easy planes, was 3–6 % of the dipolar anisotropy field. We expect that thermal-fluctuation-induced absorption peaks can be found in antiferromagnetically ordered solid ^{3}He as well. The low-field, up-up-down-down phase[4,5] has an easy-plane anisotropy and, therefore, there is a clear analogy with the type-I antiferromagnets investigated by us.

The NMR response of antiferromagnetically ordered nuclear spins in silver at nanokelvin temperatures were analyzed using the MF theory. The observed positions and intensities of the two antiferromagnetic resonances could be explained rather well; this was the case for copper, too. To conclude, we have demonstrated that numerical simulations, combined with mean-field calculations, provide a powerful tool for investigating dynamics of magnetically ordering spin systems.

ACKNOWLEDGMENTS

We thank A. S. Borovik-Romanov, O. V. Lounasmaa, K. K. Nummila, M. Steiner, G. E. Volovik and, especially, P. J. Hakonen for useful discussions. This research was sponsored by the Academy of Finland. M.T.H. acknowledges financial support by the Vilho, Yrjö, and Kalle Väisälä Foundation.

APPENDIX A: STATIC SUSCEPTIBILITY

Differentiating Eq. (3) with respect to **B**, we find for a type-I spin configuration

$$-\lambda \frac{\partial S_i^\alpha}{\partial b_\beta} = \sum_\mu \left(\delta_{\alpha\mu} - \tau \frac{S_i^\alpha S_i^\mu}{|\mathbf{S}_i|^2} \right) \left(\delta_{\mu\beta} - \sum_{\nu,j} A_{ij}^{\mu\nu} \frac{\partial S_j^\nu}{\partial b_\beta} \right). \tag{A1}$$

Here $\delta_{\alpha\beta}$ is the Kronecker symbol and we have introduced $\mathbf{S}_i = \langle \mathbf{I}_i \rangle / I$ and $\mathbf{b} = \gamma\hbar \mathbf{B}/I$, and defined a function $\tau = \tau(p)$ which can be written in a parametric form:

$$\tau[p(x)] = 1 - \frac{x}{p(x)} \frac{dp(x)}{dx}, \quad p(x) = \mathcal{B}_I(x). \tag{A2}$$

At zero temperature one has $\tau = 1$ which implies that $\mathbf{S}_i \cdot \partial \mathbf{S}_i / \partial b_\beta = 0$, consistently with the conservation of lengths $|\mathbf{S}_i| = 1$. At small polarizations $\tau \approx 0$ since p is then approximately proportional to x. In this case one obtains $\underline{\chi}(0) \approx \chi_0 \underline{I}$. Fourier transformation of Eq. (A1) yields

$$\sum_\mu \left[\delta_{\alpha\mu}(\lambda_0 - \lambda) - \tau\lambda_0 D_0^{\alpha\mu} \right] \frac{\partial m^\mu}{\partial b_\beta} - \tau \sum_{j=1}^{3} \sum_{\mu\nu} D_j^{\alpha\mu} A^{\mu\nu}(\mathbf{Q}_j) \frac{\partial d_j^\nu}{\partial b_\beta} = \delta_{\alpha\beta} - \tau D_0^{\alpha\beta} \tag{A3}$$

and

$$-\tau\lambda_0 \sum_\mu D_j^{\alpha\mu} \frac{\partial m^\mu}{\partial b_\beta} + \sum_{\mu\nu} \left[(\delta_{\alpha\mu} - \tau D_0^{\alpha\mu}) A^{\mu\nu}(\mathbf{Q}_j) - \delta_{\alpha\mu}\delta_{\mu\nu}\lambda \right] \frac{\partial d_j^\nu}{\partial b_\beta} - \tau \sum_{\mu\nu} D_k^{\alpha\mu} A^{\mu\nu}(\mathbf{Q}_l) \frac{\partial d_l^\nu}{\partial b_\beta} - \tau \sum_{\mu\nu} D_l^{\alpha\mu} A^{\mu\nu}(\mathbf{Q}_k) \frac{\partial d_k^\nu}{\partial b_\beta} = -\tau D_j^{\alpha\beta}, \tag{A4}$$

where (j,k,l) stands for (1,2,3), (2,3,1), or (3,1,2). We have written

$$\frac{S_i^\alpha S_i^\beta}{|\mathbf{S}_i|^2} = D_0^{\alpha\beta} + \sum_{j=1}^{3} D_j^{\alpha\beta} \cos(\mathbf{Q}_j \cdot \mathbf{r}_i) \tag{A5}$$

with

$$p^2 D_0^{\alpha\beta} = m^\alpha m^\beta + d_1^\alpha d_1^\beta + d_2^\alpha d_2^\beta + d_3^\alpha d_3^\beta, \tag{A6}$$

$$p^2 D_j^{\alpha\beta} = m^\alpha d_j^\beta + d_j^\alpha m^\beta + d_k^\alpha d_l^\beta + d_l^\alpha d_k^\beta. \tag{A7}$$

Indices (j,k,l) are as in Eq. (A4). The susceptibility $\chi^{\alpha\beta}(0) = \mu_0 \rho (\gamma\hbar)^2 \partial m^\alpha / \partial b_\beta$ can now be found by solving Eqs. (A5) and (A6).

The solution is slightly complicated by the fact that the equations do not fix certain linear combinations of the quantities $\partial d_j^\alpha / \partial b_\beta$; this behavior is related to the ground-state degeneracy within the MF theory. A possible way to eliminate this inconvenience is to substitute λ with $\lambda - \epsilon$ in the left-hand sides of Eqs. (A1), (A5), and (A6); the equations can be then solved and the limit $\epsilon \to 0$ taken. The physical meaning of the procedure lies in the fact that any MF ground state can be stabilized by adding a space-dependent external field, proportional to ϵ, in such a way that this field is at every site along the spin direction of the given structure. A small positive ϵ amounts thus to the assumption of a stable structure. In reality the stability is provided by certain thermal and quantum mechanical effects which are ignored in the MF description.

*Present address: Nokia Research Center, Heikkiläntie 7, P.O. Box 45, FIN-00211 Helsinki, Finland. Electronic address: Marko.Heinila@research.nokia.com

†Present address: VTT Automation, Measurement Technology, P.O. Box 1304, FIN-02044 VTT, Finland. Electronic address: Aarne.Oja@vtt.fi

[1] For reviews, see P.J. Hakonen, O.V. Lounasmaa, and A.S. Oja, J. Magn. Magn. Mater. **100**, 394 (1991); P. Hakonen and O.V. Lounasmaa, Science **265**, 1821 (1994); A.S. Oja and O.V. Lounasmaa, Rev. Mod. Phys. (to be published).

[2] J.T. Tuoriniemi, K.K. Nummila, R.T. Vuorinen, O.V. Lounasmaa, A. Metz, K. Siemensmeyer, M. Steiner, K. Lefmann, K.N. Clausen, and F.B. Rasmussen, Phys. Rev. Lett. **75**, 3744 (1995).

[3] P.J. Hakonen, R.T. Vuorinen, and J.E. Martikainen, Phys. Rev. Lett. **70**, 2818 (1993).

[4] D.D. Osheroff, M.C. Cross, and D.S. Fisher, Phys. Rev. Lett. **44**, 792 (1980).

[5] M.C. Cross and D.S. Fisher, Rev. Mod. Phys. **57**, 881 (1985).

[6] M.T. Heinilä and A.S. Oja, Phys. Rev. B **52**, R6967 (1995).

[7] S. Foner, in *Magnetism*, edited by G.T. Rado and H. Suhl (Academic, New York, 1963), p. 384.

[8] F. Keffer, in *Handbuch der Physik*, Vol. XVIII/2 (Springer Verlag, Berlin, 1966), p. 1.

[9] A.I. Akhiezer, V.G. Bar'yakhtar, and S.V. Peletminskii, *Spin Waves* (North-Holland, Amsterdam, 1968).

[10] M.T. Huiku and J.K. Soini, J. Low Temp. Phys. **50**, 523 (1982).

[11] J. Villain, R. Bidaux, J.-P. Carton, and R. Conte, J. Phys. (Paris) **41**, 1263 (1980).
[12] C.L. Henley, Phys. Rev. Lett. **62**, 2056 (1989).
[13] A.G. Gukasov, Th. Brückel, B. Dorner, V.P. Plakhty, W. Prandl, E.F. Shender, and O.P. Smirnov, Europhys. Lett. **7**, 83 (1988).
[14] M.T. Heinilä and A.S. Oja, Phys. Rev. B **50**, 15 843 (1994).
[15] P. Kumar, J. Kurkijärvi, and A.S. Oja, Phys. Rev. B **33**, 444 (1986).
[16] L.H. Kjäldman and J. Kurkijärvi, Phys. Lett. **71A**, 454 (1979).
[17] A.S. Oja, X.-W. Wang, and B.N. Harmon, Phys. Rev. B **39**, 4009 (1989).
[18] J.H. Van Vleck, J. Chem. Phys. **9**, 85 (1941).
[19] M.T. Heinilä and A.S. Oja, Phys. Rev. B **48**, 7227 (1993).
[20] M.H. Cohen and F. Keffer, Phys. Rev. **99**, 1128 (1955).
[21] D. Vollhardt and P. Wölfle, *The Superfluid Phases of Helium 3* (Taylor & Francis, London, 1990).
[22] A.J. Annila, K.N. Clausen, A.S. Oja, J.T. Tuoriniemi, and H. Weinfurter, Phys. Rev. B **45**, 7772 (1992).
[23] The quantum spin system Eq. (1) can be approximated with a classical model by substituting $\mathbf{I}_i \rightarrow I\hat{\mathbf{S}}_i$. Under this assumption, it is possible to convert the ω and χ of our scaled classical model of Eq. (41) to the real units of the quantum system. To obtain the angular frequency and susceptibility in SI system, it is necessary to multiply ω by $I/\hbar$ and χ by $\mu_0\rho(\gamma\hbar)^2$.
[24] The wave vector for which the lowest eigenvalue of $A(\mathbf{q})$ assumes its global minimum changes from type-I ordering vectors $\mathbf{Q}_j$ to wave vectors of the form $\mathbf{q}=(\pi/a)(x,x,0)$ at $J_2/J_1 \approx -0.132$ when $J_1>0$ and $D_1/J_1=0.35$. When $J_2/J_1<-0.132$, the minimum is at the type-I ordering vectors $\mathbf{Q}_j$ which correspond to $x=1$.
[25] The quoted exchange constants are consistent with various NMR measurements (Ref. 1) of silver and first-principles electronic band-structure calculations by B.N. Harmon, X.-W. Wang, and P.-A. Lindgård, J. Magn. Magn. Mater. **104-107**, 2113 (1992).
[26] We used the pseudorandom number generator given in Fig. 3 of P. L'Ecuyer, Comm. ACM **31**, 742 (1988). For a study of the properties of this generator in the context of a MC simulation of a lattice model, see P.D. Coddington, Int. J. Mod. Phys. **5**, 547 (1994). We used nonoverlapping sections of the sequence by saving the state of the generator at the end of each run and by starting from there in the beginning of the next run.
[27] S.J. Frisken and D.J. Miller, Phys. Rev. Lett. **61**, 1017 (1988).
[28] W. Minor and T.M. Giebultowicz, J. Phys. (Paris) Colloq. **49**, C8–1551 (1988).
[29] H.T. Diep and H. Kawamura, Phys. Rev. B **40**, 7019 (1989).
[30] M.T. Heinilä and A.S. Oja, Phys. Rev. B **48**, 16 514 (1993).
[31] H.E. Viertiö and A.S. Oja, in *Quantum Fluids and Solids–1989* (University of Florida), edited by G.G. Ihas and Y. Takano AIP Conf. Proc. No. 194 (AIP, New York, 1989) p. 305.
[32] H.E. Viertiö, Phys. Scr. **T33**, 168 (1990).
[33] H. Viertiö, Ph.D. thesis, Helsinki University of Technology, 1992.
[34] G.M. Wysin and A.R. Bishop, Phys. Rev. B **42**, 810 (1990).
[35] K. Chen and D.P. Landau, Phys. Rev. B **49**, 3266 (1994).
[36] R. Kubo and K. Tomita, J. Phys. Soc. Jpn. **9**, 888 (1954).
[37] To obtain $\chi(\omega)$ with the described numerical procedure, CPU time of 215 minutes was needed on a Power 2/m390 processor of the IBM SP2 system.
[38] T. Oguchi, Phys. Rev. **117**, 117 (1960).
[39] M.T. Huiku, T.A. Jyrkkiö, J.M. Kyynäräinen, M.T. Loponen, O.V. Lounasmaa, and A.S. Oja, J. Low Temp. Phys. **62**, 433 (1986).
[40] P.J. Hakonen and S. Yin, J. Low Temp. Phys. **85**, 25 (1991).
[41] P.J. Hakonen, S. Yin, and K.K. Nummila, Europhys. Lett. **15**, 677 (1991).
[42] The value $B_c = 155\ \mu$T is for a spherical sample. For a sample with a zero demagnetizing factor $B_c=140\ \mu$T, which is somewhat higher than the zero temperature $B_c=100\pm10\ \mu$T extrapolated from experiments (Refs. 2 and 41).
[43] See the data in Fig. 19 in Ref. 41. There is a misprint in the figure: the vertical axis should be I_-/I_+ instead of I_+/I_-.